Probing the Structure, Pseudorotation and Radial Vibrations of Cyclopentane by Femtosecond Rotational Raman Coherence Spectroscopy

Philipp Kowalewski, Hans-Martin Frey, Daniel Infanger, and Samuel Leutwyler*

Department of Chemistry and Biochemistry, University of Bern, Freiestrasse 3, CH-3012 Bern, Switzerland

E-mail: leutwyler@dcb.unibe.ch

Abstract

Femtosecond time-resolved Raman rotational coherence spectroscopy (RCS) is employed to determine accurate rotational, vibration-rotation coupling constants and centrifugal distortion constants of cyclopentane (C_5H_{10}). Its lowest-frequency vibration is a pseudorotating ring deformation that interconverts 10 permutationally distinct but energetically degenerate "Twist" minima interspersed by 10 "Bent" conformers. While the individual Twist and Bent structures are polar asymmetric tops, the pseudorotation is fast on the time scale of external rotation, rendering cyclopentane a fluxionally nonpolar symmetric-top molecule. The pseudorotational level pattern corresponds to a one-dimensional internal rotor with a pseudorotation constant $B_{ps} \sim 2.8$ cm^{-1}. The pseudorotational levels are significantly populated up to $l = \pm 13$ at 298 K, $< 10\%$ of the molecules are in the $l = 0$ level. The next higher vibration is the "radial" ν_{23} ring-deformation mode at 273 cm^{-1}, which is far above the pseudorotational fundamental. Fs Raman RCS measurements were performed in a gas cell at $T = 293$K and in a

*To whom correspondence should be addressed

pulsed supersonic jet at $T \sim 90$ K. The jet cooling reduces the pseudorotational distribution to $l < \pm 8$ and eliminates the population of ν_{23}, allowing to determine the rotational constant as $A_0 = B_0 = 6484.930(11)$ MHz. This value is ~ 300 times more precise than the previous value. The fit of the RCS transients reveals that the rotation-pseudorotation coupling constant $\alpha^B_{e,ps} = -0.00070(1)$ MHz is diminutive, implying that excitation of the pseudorotation has virtually no effect on the B_0 rotational constant of cyclopentane. The smallness of $\alpha^B_{e,ps}$ can be realized when comparing to the vibration-rotation coupling constant of the ν_{23} vibration, $\alpha^B_{e,23} = -9.547(1)$ MHz, which is about 10^4 times larger.

1 Introduction

Following early reports of an abnormally high entropy and heat capacity of gaseous cyclopentane,[1,2] Pitzer and collaborators interpreted this phenomenon in terms of an ultra-soft out-of-plane ring-puckering vibration, whose phase moves around the cyclopentane ring.[3–5] Starting from the "planar" D_{5h}-symmetric structure shown in Figure 1(a), the five-membered ring of cyclopentane can pucker in two ways while retaining symmetry: Any of the five methylene groups can move out of the plane, forming a flap that points up (+) or down (-), leading a *Bent* conformation of C_s-symmetry shown in Figure 1(b). Alternatively, two second-nearest methylene groups can twist relative to the others, resulting in the C_2-symmetric *Twist* structure shown in Figure 1(c).[3–5] As described by Kilpatrick et al., the *Bent* and *Twist* structures are easily interconverted along the cyclic coordinate denoted pseudorotation[3–5]

$$z_k = q_e \cdot \cos\left(\frac{4\pi}{5}k + 2\phi\right) \tag{1}$$

where q_e is the equilibrium puckering amplitude, ϕ is the phase angle of maximum amplitude and $k = 1, 2...5$ numbers the C atoms.

Starting from the *Bent* conformation B1^+ at $\phi = 0°$ shown at the left of Figure 2, increasing ϕ by $36°$ leads to the degenerate B2^- structure, and from there on to eight further B$n^\pm$ conformers

that lie at intervals of 36° along ϕ. These ten B$n^{\pm}$ forms are interspersed by 10 distinct *Twist* but degenerate conformers denoted T4^{+}, T5^{-}, T$n^{\pm}$ etc., which are shifted by $\phi = \pm 18^\circ$ relative to the *Bent* configurations. The energy difference and the barrier(s) between the *Twist* and *Bent* stationary points are so small, $V_{10} = 0.1 - 2$ cm^{-1},[6–8] that cyclopentane is free to pseudorotate over all 20 conformations, in accordance with the original Pitzer model.[3–8]

Harris et al. showed that the puckering/twisting Hamiltonian based on the coordinate in eqn. (1) can be transformed to polar coordinates $\{R, \phi\}$.[4] The two-dimensional potential energy surface (PES) is trough-like, as shown in Figure 3. The cyclic pseudorotation coordinate $\phi = 0...2\pi$ that interconverts the *Bent* and *Twist* isomers extends along the bottom of the trough.[4–8] The "radial" coordinate R in Figure 3 corresponds to a twisting vibration that planarizes both the *Bent* and *Twist* conformers. The planar D_{5h} form shown in Figure 1(a) lies at the $R = 0$ saddle point in Figure 3.[4,5] Near the minimum of the trough at R_{min}, the radial coordinate R corresponds to the ν_{23} normal mode, which is the lowest-frequency "true" vibration of the *Bent* and *Twist* isomers.

For a zero barrier between the *Bent* and *Twist* forms ($V_{10} = 0$ in Figure 2), the radial and angular parts of the Hamiltonian are exactly separable. The pseudorotation energy levels become those of a one-dimensional free internal rotor with rotational quantum number $l = 0, \pm 1, \pm 2, ...$ and with the internal-rotation energy $E_l = B_{ps} \cdot l^2$. B_{ps} is the pseudorotational constant that takes into account the reduced moment of inertia of the out-of-plane pseudorotational motion. The pseudorotation levels and wave functions for $l = 0, \pm 1, \pm 2$ are shown in Figure 2 using $B_{ps} \sim 2.8$ cm^{-1}.[6,7,9] As shown in Figure 2 the V_{10} barrier is considerably smaller than B_{ps}, so the potential energy modulation along ϕ can be neglected.[6,7,9] On the other hand, B_{ps} is much smaller than $k_B T$ at room-temperature, so many pseudorotational energy levels are thermally populated (see below), giving rise to the anomalously large vibrational entropy contribution.[1–3]

Mills derived infrared (IR) and Raman selection rules for cyclopentane using the molecular symmetry (MS) group D_{5h}, assuming free pseudorotation and a high potential hump at the D_{5h}/($R = 0$) conformation in Figure 3.[9] In a pioneering high-resolution Raman scattering experiment in 1963, Tanner and Weber determined the symmetric-top rotational constants $B_0 =$

$6475(\pm 3)$ MHz for cyclopentane and $4827(\pm 4)$ MHz for d_5-cyclopentane.[10] The rotational Raman signal of cyclopentane is small because of its relatively small polarizability anisotropy, and Tanner and Weber had to conduct their gas-cell experiments at $p = 1$ atmosphere and $T \sim 328$ K to obtain a useful Raman signal.[10] Durig and Wertz analyzed a number of sharp Q-branches associated with the 1460 cm^{-1} IR band of cyclopentane and identified these as pseudorotational sequence bands.[6] From their analysis of the pseudorotational constant they estimated an average out-of-plane amplitude of the C atoms as $q_e = 0.48$ Å.[6] Based on vibrational Raman spectra of gaseous cyclopentane from $200 - 330$ cm^{-1}, Carreira et al. recalculated the central barrier be 1824 ± 50 cm^{-1} and the out-of-plane amplitude to be $q_e = 0.47 \pm 0.025$ Å .[11] Bauman and Laane investigated normal (d_0)-cyclopentane and its d_1-, d_2-, d_6- and d_{10}- deuterated derivatives with respect to their pseudorotational and radial motions.[7] They determined pseudorotational constants for the isotopomers d_0 ($B_{ps} = 2.8 - 2.9$ cm^{-1}), d_1 ($B_{ps} = 2.45$ cm^{-1}) and d_{10} ($B_{ps} = 1.85$ cm^{-1}).[7] More recently, Ocola et al. complemented additional IR and Raman spectra of cyclopentane with DFT calculations and with high-level structure calculations using the coupled-cluster singles and doubles method with perturbative treatment of triple excitations [CCSD(T)] and the cc-pVTZ basis set.[8] These predict the *Twist* to be the lower-energy form, with the *Bent* conformer barely 1 cm^{-1} above.[8]

Rotational coherence spectroscopy (RCS) is a time-domain spectroscopic method,[12–14] which, unlike microwave and millimeter-wave spectroscopic methods,[15,16] can also be applied to nonpolar molecules.[17–33] We have shown for several nonpolar linear and symmetric tops such as CS_2, cyclopropane to cyclohexane, cyclooctatetraene, 1,3,5-trifluorobenzene and hexafluorobenzene that the rotational constants can be determined with a relative accuracy of $\sim 10^{-6}$ if the RCS signal contributions from low-lying thermally populated excited vibrations are taken into account.[27–34] We have also determined semiexperimental equilibrium (r_e) C-C and C-F bond lengths in the above molecules.

For cyclopentane with its large number of low-energy pseudorotational levels, the temperature effects on the rotational Raman RCS signal are enormous. Cooling the sample in a supersonic

jet strongly reduces the vibrational and rotational temperatures, and the comparison with room-temperature RCS spectra[33,34] allowing one to observe the coupling of the pseudorotational and the ν_{23} radial vibrations to the rotational constants. The adiabatic jet expansion also increases the time between collisions beyond the experimental time scale of ~ 5 ns, effectively eliminating the J- and M_J-dephasing collisions that lead to a loss of RCS signal.[17,18,23,35]

2 Methods

The experimental setup for recording femtosecond rotational Raman rotational coherence transients in a gas cell[29–31] and its extension to a pulsed supersonic-jet source have been described earlier.[33] The experimental setup is shown in Figure 4, details are given in the Supporting Information. Similar to our previous RCS work on cyclohexane,[32,33] the supersonic-jet experiments are performed about 5 nozzle diameters downstream of the nozzle ($x/D \sim 5$ with $D = 0.4$ mm). Also, relatively high cyclopentane concentrations had to be employed (55 %) to get a reasonable signal/noise ratio. For both reasons, the rotational temperature T_{rot} is relatively high (see section 4.1).

Correlated ab initio calculations were performed with the MP2 and CCSD(T) methods using Dunning's cc-pVDZ and cc-pVTZ basis sets; all electrons were correlated. The cyclopentane geometries were optimized with analytic gradient methods. Harmonic and cubic force fields were computed using analytical second derivative techniques.[36] The symmetries of the *Bent* (C_s), *Twist* (C_2) and of the D_{5h} planar structures were Z-matrix defined; symmetry was continuously enforced during the geometry optimization. For the Cartesian coordinates of the *Bent* and *Twist* CCSD(T)/cc-pVTZ optimized structures, see the Supporting Information. All calculations were carried out using the CFOUR program package.[37]

3 Degenerate four-wave mixing theory and RCS signal analysis

3.1 Modeling the degenerate four-wave mixing signal

The theory and simulation of fs rotational Raman RCS transients detected by degenerate four-wave mixing (DFWM) has been previously given.[31] Briefly, three laser beams of equal intensity and polarization are focused into the Raman-active medium using a folded Boxcar arrangement. After a time lag t, the anisotropy, which is induced at time $t = 0$ by the pump and dump pulses (with electric fields E_1,E_2), is probed via the probe pulse (E_3). For off-resonant excitation, the time-dependent degenerate four-wave mixing (DFWM) signal intensity is given by:

$$I_{DFWM}(t) = \int_{-\infty}^{\infty} G(\tau) \left|\chi^{(3)}(t-\tau)\right|^2 \mathrm{d}\tau \tag{2}$$

Prior to each RCS experiment the experimental apparatus function $G(t)$ is measured via the zero time Kerr-peak of Ar gas. The stimulated Raman response of the medium to the three laser pulses is described by the third-order susceptibility $\chi^{(3)}(t)$, which can be modeled for $t > 0$ as:

$$\chi^{(3)}(t) = C \sum_{J,K,v} \left[b_{J,K,v} \sin\left(\Delta\omega_{J,K,v} t\right)\right] \tag{3}$$

where C is a proportionality constant, $b_{J,K,v}$ is an amplitude coefficient that includes the rotational and vibrational level population factors, the rotational ($g_{J,K}$) and vibrational (g_v) degeneracies, nuclear-spin statistics and the rotational Raman intensity coefficients for anisotropic Raman scattering (Placzek-Teller factors).[38–41]

$$b_{J,K,v} = g_{J,K,v} \cdot p_{J,K,v} \cdot b^{JK}_{J'K'} \tag{4}$$

The $\Delta\omega_{J,K,v}$ in eqn. (3) are the frequencies of all rotational Raman-allowed transitions from states with rotational quantum numbers J, K and vibrational quantum number v that can undergo stimulated Raman transitions within the fs laser bandwidth of $\sim$ 100 cm^{-1}. While the

classical *Bent* and *Twist* equilibrium geometries are asymmetric, the vibrational $v = 0$ level is delocalized over all 20 stationary points, see Figure 2, which renders cyclopentane an effective *symmetric*-top molecule. Therefore, the rotational energy levels and Raman frequencies $\Delta\omega_{J,K,v} = |E_{rot,J',K',v} - E_{rot,J,K,v}|/\hbar$ were calculated using the symmetric oblate-top equation including quartic centrifugal distortion:[42]

$$E_{rot,J,K,v} = B_v J(J+1) + (C_v - B_v) K^2 - D_{J,v} J^2 (J+1)^2 - D_{J,K,v} J(J+1) K^2 - D_{K,v} K^4 \quad (5)$$

The rotational constants B_v and C_v are vibration-dependent, e.g. the rotational constant $B_{v,i}$ of the i-th vibration is

$$B_{v,i} = B_e - \sum \alpha_{e,i}^{B} (v_i + d_i/2) \quad (6)$$

where B_e is the equilibrium rotational constant, $\alpha_{e,i}^{B}$ are the vibration-rotation interaction constants associated with each vibration, v_i is the quantum number of the i-th vibration and $d_i = 1$ or 2 is the vibrational degeneracy. The rotational constant C_v and the centrifugal distortion constant $D_{K,v}$ cancel for rotational Raman transitions and cannot be determined experimentally; they are taken from the CCSD(T)/cc-pVXZ calculations.

In the gas-cell measurement, collisions that change the phase of $\chi^{(3)}(t)$ destroy the rotational coherence of the sample with increasing delay time t. We model these effects by modifying eqn. (3) according to the energy gap law for collision-induced rotational energy transfer (RET):[43,44]

$$p_{coll}{}_{J'K'}^{JK} = exp\left(-a \cdot t \cdot exp\left(-b \cdot \Delta E_{J'K'}^{JK}\right)\right) \quad (7)$$

where a denotes the probability of a collision per time unit, b the probability of an energy transfer per energy unit induced by a collision, and $E_{J'K'}^{JK}$ is the rotational energy spacing. In this work both a and b are fit parameters.

4 Results and Discussion

4.1 Raman RCS jet measurements, fitting and rotational constants of C_5H_{10}

The experimental RCS transients of jet-cooled cyclopentane are shown in Figure 5 from recurrence #17 to recurrence #34.5 and in 6 from recurrence #34 to recurrence #51.5; note that the recurrences are normalized to the same maximum height. The peak signal actually decreases slowly with increasing delay time t because of the slight spreading of the later recurrences due to centrifugal distortion effects, i.e., the low-J levels contribute more strongly to the early part of the recurrence and the high-J levels to the later part.[32,33] This is seen especially clearly when comparing the half-integer recurrences, e.g., recurrence #17.5 in Figure 5 with #51.5 in Figure 6. In contrast to the integer recurrences, which contain interfering contributions from $\Delta J = +1$ as well as $\Delta J = +2$ transitions, the half-integer recurrences involve only $\Delta J = +2$ rotational Raman transitions.[14] Their maximum height is typically $40 - 45$ % of the neighboring integer recurrences.

For the supersonic-jet measurements we originally defined independent rotational, vibrational and pseudorotational Boltzmann distributions allowing different effective temperatures, but the fitted rotational, pseudorotational and vibrational temperatures were found to agree closely, $T_{rot} = T_{vib} = T_{ps} = 89 \pm 3$ K. Although these temperatures might seem high, note that we need to work close to the supersonic-jet nozzle at $x/D \sim 5$, see section 2. The T_{rot} for cyclopentane is similar to the $T_{rot} = 80 \pm 3$K for cyclohexane in a He expansion[33] and considerably lower than the $T_{rot} = 130 \pm 5$K recently determined for para-difluorobenzene in an Ar expansion.[45]

Table 1 lists the calculated pseudorotational and radial vibrational level populations of cyclopentane at the experimental temperatures $T = 90$ K and 295 K. Table 1 shows that at $T = 90$ K the ν_{23} ($r = 1$) and its associated pseudorotational levels contribute $< 1\%$ to the vibrational population and hence $\leq 1 \cdot 10^{-4}$ to the RCS signal according to eqn. (2). This allows one to disregard the signal contributions from these levels – and *a forteriori* those of the higher-frequency vibrations – to the simulated RCS trace and the fit. Similarly, the pseudorotational states built on the $r = 0$ level only need to be considered up to about $l = 8$. The centrifugal distortion constants D_J and D_{JK} are

more accurately determined at room temperature because of the larger high-J population, hence they were set to the gas-cell values, which are derived in the following section. Summarizing, the supersonic-jet fits yield the ground-state rotational constant B_0 and the rotational constants of the pseudorotationally excited levels, which are collectively described by the pseudorotation-rotation interaction constant $\alpha^B_{ps,e}$ in combination with eqn. (6).

We recorded the RCS transient with a step size of 26.69 fs over 4 ns, divided into 15 sets of five and a half consecutive recurrences. Each set was measured three times. Sets for which the average laser power was stable within $\pm 1\%$ were collated and fitted together; this procedure greatly improves the fit accuracy of the B_0 when compared to fitting single recurrences. Using the fit model described in section 3.1 each transient was least-squares fitted using a Levenberg-Marquardt algorithm. The mean value of the $N = 15$ sections for $B_{0,N}$ is $\bar{B}_0 = 6484.930$ MHz. Since we are interested in the parameter values averaged over all 15 sections, the appropriate error is the error of the mean, $\sigma_{\bar{x}} = \sigma_x/\sqrt{N}$, giving $\sigma_{\bar{B}_0} = 0.011$ MHz.

4.2 Gas cell RCS measurements of C_5H_{10}

Figure 7 shows a section of the RCS transient measured in the gas cell. Again the maxima of the recurrences are normalized to the same value. Table 1 shows that the population of the pseudorotational and radial levels increases strongly at 293 K. As the number of associated Raman transitions and the spread in Raman transition frequencies increase, the temporal modulations within the recurrences become much more rapid. This is clearly observed when comparing Figure 7 with Figure 5, which are plotted on the same delay time scale. Additionally to the spreading caused by the centrifugal distortion on higher-J states, collisional dephasing is much more important in the cell compared to the supersonic jet, since the collision probabilities and the associated energy transfers increase.

We fitted the gas-cell room-temperature RCS transient for the parameters that depend on levels which are *not* strongly populated at 90 K, i.e., the centrifugal distortion constants D_J and D_{JK} and the rotational-vibrational coupling constant α^B_{23} of the ν_{23} $r = 1$ radial level. B_0 was retained from

the supersonic-jet measurement, as discussed above. Because of the mutual interdependence of the parameters (D_J and D_{JK} from the room-temperature fit are needed for the supersonic-jet fit and B_0 is needed for the gas-cell fit) the two parameter sets were fitted until they were mutually consistent. Sections of three and a half consecutive recurrences were recorded three times. These were collated into series of 2 half and 2 full recurrences, giving 17 sections over the range from recurrence #13 to #34.5. As described before each of the $n = 17$ sections were fitted; the corresponding results are listed in the lower part of Table 2.

5 Discussion

The supersonic cooling to $T \sim 90$ K allows one to determine the ground-state rotational constant as $B_0 = 6484.93 \pm 0.01$ MHz (1σ error estimate), corresponding to a relative accuracy of $2 \cdot 10^{-6}$. Our B_0 is about 300 times more accurate than the $B_0 = 6475 \pm 3$ MHz measured by Tanner and Weber in their pioneering cw resolution Raman scattering experiment in 1963.[10] The two values differ by only 0.15%, attesting to the high accuracy of those early experiments.[10] We ascribe the difference to the higher temperature and pressure ($p = 1$ atmosphere and $T \sim 328$ K) in the experiments of Tanner and Weber, which was necessary because of the weak rotational Raman scattering of cyclopentane.[10]

The influence of the pseudorotational motion on the rotational constant is described by the vibration-rotation coupling parameters $\alpha^B_{e,i}$ in eqn. 6. These corrections are calculated at the second-order perturbation theoretical (PT2) level implemented in CFOUR.[37] The CCSDT/cc-pVTZ calculated pseudorotation-rotation coupling constants are $\alpha^B_{ps} = -0.937$ MHz for the *Bent* conformer and -0.538 MHz for the *Twist* conformer, see Table 2. These are ~ 10 times smaller that the calculated and the experimentally observed *vibration*-rotation $\alpha^B_{e,i}$ values for the low-frequency vibrations of cyclobutane and cyclohexane, which are of the order of $3-10$ MHz.[28,29,32,33] However, the experimental pseudorotation-rotation coupling constant of cyclopentane α^B_{ps} is only -0.00070 MHz! This implies that excitation of the pseudorotational motion has virtually no effect

on the $A_0 = B_0$ rotational constant of cyclopentane. That the experimental α_{ps}^B differs by a factor of ~ 1000 from the calculated value is not so surprising, since PT2 is not appropriate for such a large-amplitude motion.

Tanner and Weber analyzed their B_0 rotational constants based on the assumption that cyclopentane possesses D_{5h} symmetry in its equilibrium configuration (although they also mentioned "a slight aplanarity of the carbon ring") and deduced an equilibrium C-C bond length r_e(C-C)$= 1.537(2)$ Å.[10] Later work has made it clear that the D_{5h} symmetric planar structure of cyclopentane is in fact a high-energy form of little physical significance: Table 3 shows that the CCSD(T)/cc-pVTZ energy of the D_{5h}-symmetric stationary point is 2100 cm^{-1} above the *Twist* (C_2) form. At the same computational level, the calculated energy difference between the *Twist* and the *Bent* forms is only 0.05 cm^{-1}, see also ref. 8

Below, we will interpret the calculated geometries of the *Bent* and *Twist* limiting structures in a manner that is consistent with the experimental B_0 rotational constant, but the following analysis should not be taken to imply that the *Bent* and *Twist* equilibrium structures are separately observable in our experiments. The *Bent* (C_s) and *Twist* (C_2) forms in Figure 1(b,c) exhibit three different C-C bond lengths. Using the C atom numbering in Figure 1(b,c) one sees that the C1-C2 and C1-C5 bonds length are symmetrically equal, the C2-C3 and C4-C5 bonds are also equal (albeit different from the first pair), while the C3-C4 bond length is unique in both conformers.

We first discuss the equilibrium rotational constants and the vibrationally averaged rotational constants of the distinct *Bent* and *Twist* minima. The A_e and B_e equilibrium rotational constants were calculated at the CCSD(T)-cc-pVTZ level and are reported in lines 1 and 2 of Table 2. The slight differences between A_e and B_e that occur for both *Bent* and *Twist* reflects the fact that neither structure corresponds to a symmetric top. The A_e, B_e equilibrium rotational constants are then corrected for the rotation–vibration interaction, corresponding to the summation over the $\alpha_{e,i}^B$ term in eqn.(6). The rotation-vibration corrected A_0 and B_0 constants of the *Bent* and *Twist* forms are given in lines 3 and 4 of Table 2.

In the second step, we consider the effect of the rapid pseudorotational averaging, but assuming

that the *Bent* structure is averaged only over its 10 equivalent (permutationally distinct) $B_n^{\pm}$ forms. This averages the rotational constants $A_0(B_n^{\pm})$ and $B_0(B_n^{\pm})$ to are averaged, giving rise to the *effective* symmetric-top rotational constant $(A_0 + B_0)/2 = 6489.864$ MHz, see line 5 in Table 2. Analogously, we assume that the pseudorotation interconverts the *Twist* structure only over its ten equivalent but distinct $T_n^{\pm}$ forms, thereby averaging the $A_0(T_n^{\pm})$ and B_0 $(T_n^{\pm})$ rotational constants to the *Twist* effective symmetric-top constant $(A_0 + B_0)/2 = 6490.11$ MHz (see Table 2). Note that the pseudorotationally averaged $(A_0 + B_0)/2$ constants of the *Bent* and *Twist* forms at this point are still distinct, reflecting the different equilibrium geometries of the two distinct stationary points. However, their rotation–vibration and pseudovibrationally averaged rotational constants differ by only 0.250 MHz or 0.004 %.

In the third step, we discuss why the *Bent* and *Twist* can be averaged. As discussed above the pseudorotation can be transformed from eqn. (1) to mass-weighted coordinates and then to polar coordinates R, ϕ, allowing to express the two-dimensional vibrational wave function as a product of radial and angular functions, $\Psi(\rho, \phi) = R(\rho) \cdot \Phi(\phi)$.[4,5] Since the V_{10} barrier between the *Bent* and *Twist* conformers is substantially lower than the $l = 0$ pseudorotational level the pseudorotational eigenfunctions are one-dimensional free-rotor functions, see Figure 2:

$$\Phi(\phi) = \frac{1}{\sqrt{2\pi}} \cdot e^{il\phi} \tag{8}$$

Eqn. (8) shows that the angular probability density distribution, given by $|\Phi(\phi)|^2$, is *independent* of ϕ and of the quantum number l for all pseudorotational eigenfunctions. Thus the *Bent* and the *Twist* structures and all structures intermediate between these two are equally weighted by the pseudorotation, independent of l. Given that the *Bent* and *Twist* values of $(A_0 + B_0)/2$ differ by so little, it is reasonable to directly average their rotational constants, instead of (more correctly) averaging their respective moment-of-inertia tensors and converting these to rotational constants. This average of the *Bent* and *Twist* calculated $(A_0 + B_0)/2$ values, given in line 6 of Table 2, can then be usefully compared to the experimental rotational constant $A_0 = B_0$ of pseudorotating

cyclopentane.

Eqn. (8) also helps to explain the minute pseudorotation-rotation coupling constant $\alpha_{ps}^{B} = -0.00070$ MHz discussed above: Since the weighting of the different *Bent* and *Twist* forms does not depend on the pseudorotational angle ϕ, all *Bent* and *Twist* forms contribute equally to the pseudorotationally averaged B_0. Since the weighting does not depend on the pseudorotation quantum number l, the pseudorotation-rotation coupling constant should be extremely small, as is in fact observed.

We now determine the equilibrium (r_e) C-C bond lengths using semi-experimental methods[36,46–49] and a basis-set extrapolation technique that we have introduced previously.[29,30,33,34] We apply this technique to the determination of the C-C bond distances, using (B_e, r_e) and (B_0, r_e) points calculated with the CCSD(T) method and the cc-pVXZ, (X = D,T) basis sets. Figure 8 plots the calculated $(A_e + B_e)/2$ and $(A_0 + B_0)/2$ rotational constants of the *Bent* and *Twist* forms of cyclopentane vs. the respective C-C equilibrium bond lengths. Separate graphs are shown for the three distinct equilibrium bond lengths C1-C2, C2-C3 and C3-C4. The upper (dashed) lines connect the double- and triple-zeta (B_e, r_e) points calculated for the respective equilibrium structures. These lines are then shifted downwards by the vibration-rotation interaction constants $\Delta = B_e - B_0$, see eqn. (6), which were calculated at the CCSD(T)/cc-pVTZ level, yielding analogous lines for the vibrationally averaged ground-state constant B_0 (full red lines). The intersections of the $B_{0,calc}$ lines with the experimental B_0 (red horizontal line) yields the experimental estimates of the r_e(C-C) equilibrium bond lengths. From these plots, one observes that:

(1) In the *Bent* and *Twist* conformers, the longest, the middle and the shortest C-C bonds exhibit similar lengths, differing by 0.005 Å at most.

(2) In the *Bent* structure, the C1-C2/C1-C5 pair constitute the shortest bonds (1.528 Å), while the same two bonds in the *Twist* structure are the longest (1.547 Å).

(3) In the *Bent* structure, the C2-C3/C4-C5 pair are of intermediate length (1.538 Å), the same pair of bonds in the *Twist* structure are also of intermediate length (1.531 Å).

(4) The unique C3-C4 bond is the longest bond (1.552 Å) in the *Bent* conformer, but constitutes

the shortest (1.527 Å) C-C bond in the *Twist* conformer.

One should not take points (2) and (4) to mean that the C-C bond lengths undergo bond length changes of up to 0.025 Å during a single step of the pseudorotation. When analyzing the individual pseudorotation steps and accounting for the label permutations of the C atoms, as shown in Figure 9, one sees that the bond length change per step is less than half that value. Figure 9 shows the first four steps of the pseudorotation in the sequence defined in Figure 2; note that in each step the C1 atom *label* rotates counter-clockwise by two C-atoms. During the first step $B_1^+ \rightarrow T_4^+$ the C1-C5 and the C4-C5 bonds expand by 0.003 and 0.009 Å, while the C2-C3 and the C3-C4 bonds contract by -0.007 Å and -0.005 Å; the C1-C2 bond length remains nearly unchanged (-0.001 Å). During the second step $T_4^+ \rightarrow B_2^-$ two bond expansions and two contractions occur which are permutations of those in the $B_1^+ \rightarrow T_4^+$ step. Thus the largest change of any C-C bond length per pseudorotation step is ± 0.009 Å.

When comparing to the unstrained C-C bond length of ethane $r_e = 1.522(1)$ Å,[50] one sees that the shortest C-C bond(s) with $r_e = 1.527 - 1.528$ Å in *Bent* and *Twist* cyclopentane are relatively unstrained. They are also very close to the C-C equilibrium bond length of cyclohexane, $r_e = 1.526(1)$ Å.[32,33] However, the ring strain in cyclopentane increases the two C-C bonds of intermediate length by $0.009 - 0.016$ Å. The most strained C-C bond(s) is (are) $0.025 - 0.030$ Å longer than the ethane r_e C-C bond length.

6 Conclusions

Femtosecond rotational Raman rotational coherence spectroscopy was performed on cyclopentane cooled in a seeded supersonic jet to $T \sim 90$ K and in a gas cell at $T = 293$ K. The former allowed to record rotational coherence transients over delay times up to ~ 4 ns. The small signal decrease over such a long delay time shows that collisional dephasing is strongly reduced in the supersonic jet, in strong contrast to gas cell experiments.[32,33]

The supersonic cooling to $T \sim 90$ K allows to determine the ground-state rotational constant as

$B_0 = 6484.93 \pm 0.01$ MHz ($\pm 1\sigma$ error estimate), corresponding to a relative accuracy of $2 \cdot 10^{-6}$. Our B_0 is 0.15% larger and about 300 times more accurate than the $B_0 = 6475(\pm 3)$ MHz measured by Tanner and Weber by high-resolution cw rotational Raman spectroscopy in 1963.[10] The small difference of 0.15 % between the two values might reflect temperature and pressure broadening effects ($p = 1$ atmosphere and $T \sim 328$ K) in the gas-cell experiment of reference 10, and attests to the high quality of the previous measurements.

Although the CCSD(T)/cc-pVTZ calculations predict that the interaction of the external molecular rotation of cyclopentane with its soft pseudorotational motion is large, resulting in a large vibration-rotation interaction constant $\alpha^B_{e,ps} = 0.5 - 0.9$ MHz, the fit to the RCS measurement showed this parameter to be ~ 1000 times smaller than calculated, i.e., -0.00070 MHz. Based on the accurate B_0, the gas-cell data could also be fitted to yield the vibration-rotation interaction constant $\alpha^B_{23} = -9.54$ MHz of the "radial" vibration ν_{23}. This value is 13000 times larger than α^B_{ps}.

The centrifugal distortion parameters D_J and D_{JK} were also measured, they agree with the CCSD(T)/cc-pVTZ prediction to within 10 %. Measuring the same molecule at two different temperatures as well as with/without collisional dephasing provides a powerful approach to increase the accuracy of the rotational and centrifugal distortion constants. The statistical correlation between the B_0 constant and the centrifugal distortion constants D_J and D_{JK} can thereby be markedly decreased.

The value for B_0 was combined with CCSD(T)/cc-pVXZ (X=D, T) calculations to determine the semi-experimental C-C equilibrium bond lengths of the *Bent* (C_s symmetric) and the *Twist* (C_2 symmetric) forms of cyclopentane. Both isomers exhibit three C-C bonds with significantly different equilibrium (r_e) bond lengths, which are calculated to be 1.527, $1.531 - 1.538$ and $1.547 - 1.552$ Å. When comparing to the unstrained C-C bond length of ethane $r_e = 1.522(1)$ Å,[50] the ring strain in cyclopentane increases two of the C-C bond lengths by 0.016 Å, and the longest C-C bond(s) by $0.025 - 0.030$ Å relative to the ethane r_e value.

Acknowledgments

Financial support from the Swiss National Science Foundation (SNSF) through grants no. 200020-144490 and 200020-130376 is gratefully acknowledged.

Supporting Information Available: A section with experimental details, a diagram of the pseudorotational-radial eigenvalues as a function of the potential shape, and the Cartesian coordinates of the CCSD(T)/cc-pVTZ geometries.This information is available free of charge via the Internet at http://pubs.acs.org.

References

(1) Douslin, D. R.; Huffman, H. M. The Heat Capacities, Heats of Transition, Heats of Fusion and Entropies of Cyclopentane, Methylcyclopentane and Methylcyclohexane. *J. Am. Chem. Soc.* **1946**, *68*, 173–176.

(2) Spitzer, R.; Pitzer, K. S. The Heat Capacity of Gaseous Cyclopentane, Cyclohexane and Methylcyclohexane. *J. Am. Chem. Soc.* **1946**, *68*, 2537–2538.

(3) Kilpatrick, J. E.; Pitzer, K. S.; Spitzer, R. The Thermodynamics and Molecular Structure of Cyclopentane. *J. Am. Chem. Soc.* **1947**, *69*, 2483–2488.

(4) Harris, D. O.; Engerholm, G. G.; Tolman, C. A.; Luntz, A. C.; Keller, R. A.; Kim, H.; Gwinn, W. D. Ring Puckering in Five-Membered Rings. I. General Theory. *J. Chem. Phys.* **1969**, *50*, 2438–2445.

(5) Ikeda, T.; Lord, R. C.; Malloy, T. B.; Ueda, T. Far-Infrared Spectra of Ring Compounds. VIII. The Effect of a Finite Central Barrier on Pseudorotation in Five-Memberde Rings. *J. Chem. Phys.* **1972**, *56*, 1434–1439.

(6) Durig, J. R.; Wertz, D. W. Vibrational Spectra and Structure of Small-Ring Compounds. X. Spectroscopic Evidence for Pseudorotation in Cyclopentane. *J. Chem. Phys.* **1968**, *49*, 2118–2121.

(7) Bauman, L. E.; Laane, J. Pseudorotation of Cyclopentane and Its Deuterated Derivatives. *J. Phys. Chem.* **1988**, *92*, 1040–1051.

(8) Ocola, E. J.; Bauman, L. E.; Laane, J. Vibrational Spectra and Structure of Cyclopentane and its Isotopomers. *J. Phys. Chem. A* **2011**, *115*, 6531–6542.

(9) Mills, I. M. Infra-Red and Raman Selection Rules for Cyclopentane. *Mol. Phys.* **1971**, *20*, 127–138.

(10) Tanner, K.; Weber, A. The Pure Rotational Raman Spectrum of Cyclopentane-d_0 and Cyclopentane-d_{10}. *J. Mol. Spectrosc.* **1963**, *10*, 381–398.

(11) Carreira, L. A.; Jiang, G. J.; Person, W. B.; Willis, J. N. Spectroscopic Determination of Barrier to Planarity in Cyclopentane. *J. Chem. Phys.* **1972**, *56*, 1440–1443.

(12) Felker, P. M.; Zewail, A. H. Purely Rotational Coherence Effect and Time-Resolved sub-Doppler Spectroscopy of Large Molecules. I. Theoretical. *J. Chem. Phys.* **1987**, *86*, 2460–2482.

(13) Felker, P. M. Rotational Coherence Spectroscopy: Studies of the Geometries of Large Gas-Phase Species by Picosecond Time-Domain Methods. *J. Phys. Chem.* **1992**, *96*, 7844–7857.

(14) Felker, P. M.; Zewail, A. H. In *Femtosecond Chemistry*; Manz, J., Wöste, L., Eds.; VCH: Weinheim, 1995; Vol. I; Chapter 5.

(15) Gordy, W.; Cook, R. L. *Microwave Molecular Spectra*, 3rd ed.; Wiley-Interscience: New York, 1984.

(16) Townes, C. H.; Schawlow, A. L. *Microwave Spectroscopy*; Dover Publications (reprint edn.): New York, 1975.

(17) Frey, H.-M.; Beaud, P.; Gerber, T.; Mischler, B.; Radi, P. P.; Tzannis, A. P. Femtosecond Nonresonant Degenerate Four-Wave Mixing at Atmospheric Pressure and in a Free Jet. *Appl. Phys. B* **1999**, *68*, 735–739.

(18) Frey, H. M.; Beaud, P.; Gerber, T.; Mischler, B.; Radi, P. P.; Tzannis, A. P. Determination of Rotational Constants in a Molecule by Femtosecond Four-Wave Mixing. *J. Raman Spectrosc.* **2000**, *31*, 71–76.

(19) Riehn, C.; Weichert, A.; Brutschy, B. Probing Benzene in a New Way: High-Resolution Time-Resolved Rotational Spectroscopy. *J. Phys. Chem. A* **2001**, *105*, 5618–5621.

(20) Frey, H. M.; Müller, A.; Leutwyler, S. Femtosecond Degenerate Four-Wave Mixing of Pyridine and Its Biologically Relevant Derivatives. *J. Raman Spectrosc.* **2002**, *33*, 855–860.

(21) Hobza, P.; Riehn, C.; Weichert, A.; Brutschy, B. Structure and Binding Energy of the Phenol Dimer: Correlated *Ab Initio* Calculations Compared with Results from Rotational Coherence Spectroscopy. *Chem. Phys.* **2002**, *283*, 331–339.

(22) Matylitsky, V. V.; Jarzęba, W.; Riehn, C.; Brutschy, B. Femtosecond Degenerate Four-Wave Mixing Study of Benzene in the Gas Phase. *J. Raman Spectrosc.* **2002**, *33*, 877–883.

(23) Jarzęba, W.; Matylitsky, V. V.; Riehn, C.; Brutschy, B. Rotational Coherence Spectroscopy of Jet-Cooled Molecules by Femtosecond Degenerate Four-Wave Mixing: Non-Rigid Symmetric and Asymmetric Tops. *Chem. Phys. Lett.* **2003**, *368*, 680–689.

(24) Riehn, C.; Matylitsky, V. V.; Jarzęba, W.; Brutschy, B.; Tarakeshwar, P.; Kim, K. Insights Into the Structure of Cyclohexane from Femtosecond Degenerate Four-Wave Mixing Spectroscopy and *Ab Initio* Calculations. *J. Am. Chem. Soc.* **2003**, *125*, 16455–16462.

(25) Kummli, D. S.; Frey, H. M.; Keller, M.; Leutwyler, S. Femtosecond Degenerate Four-Wave Mixing of Cyclopropane. *J. Chem. Phys.* **2005**, *123*, 054308.

(26) Riehn, C.; Matylitsky, V. V.; Gelin, M. F.; Brutschy, B. Double Hydrogen Bonding of Acetic Acid Studied by Femtosecond Degenerate Four-Wave Mixing. *Mol. Phys.* **2005**, *103*, 1615–1623.

(27) Kummli, D. S.; Frey, H. M.; Leutwyler, S. Femtosecond Degenerate Four-wave Mixing of Carbon Disulfide: High-Accuracy Rotational Constants. *J. Chem. Phys.* **2006**, *124*, 144307–1–7.

(28) Kummli, D. S.; Frey, H. M.; Leutwyler, S. High-Accuracy Structure of Cyclobutane by Femtosecond Rotational Raman Four-Wave Mixing. *J. Phys. Chem. A* **2007**, *111*, 11936–11942.

(29) Kummli, D. S.; Lobsiger, S.; Frey, H. M.; Leutwyler, S.; Stanton, J. F. Accurate Determination of the Structure of Cyclooctatetraene by Femtosecond Rotational Coherence Spectroscopy and *Ab Initio* Calculations. *J. Phys. Chem. A.* **2008**, *112*, 9134–9143.

(30) Kummli, D. S.; Frey, H.-M.; Leutwyler, S. Accurate Determination of the Structure of 1,3,5-Trifluorobenzene by Femtosecond Rotational Raman Coherence Spectroscopy and *Ab Initio* Calculations. *Chem. Phys.* **2010**, *367*, 36–43.

(31) Frey, H.-M.; Kummli, D.; Lobsiger, S.; Leutwyler, S. In *Handbook of High-Resolution Spectroscopy*; Quack, M., Merkt, F., Eds.; John Wiley & Sons Ltd: Chichester, UK, 2011; p 1237.

(32) Brügger, G.; Frey, H.-M.; Steinegger, P.; Balmer, F.; Leutwyler, S. Accurate Determination of the Structure of Cyclohexane by Femtosecond Rotational Coherence and *Ab Initio* Calculations. *J. Phys. Chem. A* **2011**, *115*, 9567–9578.

(33) Brügger, G.; Frey, H.-M.; Steinegger, P.; Kowalewski, P.; Leutwyler, S. Femtosecond Rotational Raman Coherence Spectroscopy of Cyclohexane in a Pulsed Supersonic Jet. *J. Phys. Chem. A* **2011**, *115*, 12380–12389.

(34) Den, T. S.; Frey, H. M.; Leutwyler, S. Accurate Rotational Constant and Bond Lengths of Hexafluorobenzene by Femtosecond Rotational Raman Coherence Spectroscopy and Ab Initio Calculations. *J. Chem. Phys.* **2014**, *141*, 194303–1–9.

(35) Brown, E. J.; Zhang, Q.; Dantus, M. Femtosecond Transient-Grating Techniques: Population and Coherence Dynamics Involving Ground and Excited States. *J. Chem. Phys.* **1999**, *110*, 5772–5788.

(36) Puzzarini, C.; Stanton, J. F.; Gauss, J. Quantum-Chemical Calculation of Spectroscopic Parameters for Rotational Spectroscopy. *Int. Rev. Phys. Chem.* **2010**, *29*, 273–367.

(37) Stanton, J. F.; Gauss, J.; Harding, M. E.; Szalay, P. G.; Auer, A. A.; J, B. R.; Benedikt, U.; Berger, C.; Bernholdt, D. E.; Bomble, Y. J.; et al., CFOUR, a quantum chemical program package. For the current version, see http://www.cfour.de.

(38) Altmann, K.; Strey, G. Application of Spherical Tensors and Wigner 3-j Symbols to the Calculation of Relative Intensities of Rotational Lines in Raman Bands of Molecular Gases. *J. Mol. Spectrosc.* **1972**, *44*, 571–577.

(39) Hegelund, F.; Rasmussen, F.; Brodersen, S. The Selection Rules and the Transition Moment for Rotation-Vibrational Transitions in Axial Molecules. *J. Raman Spectrosc.* **1973**, *1*, 433–453.

(40) Brodersen, S. In *Topics in Current Physics: Raman Spectroscopy of Gases and Liquids*; Weber, A., Ed.; Springer Verlag: Berlin, 1978; Chapter 2, pp 7–69.

(41) Weber, A. In *Handbook of High-Resolution Spectroscopy*; Quack, M., Merkt, F., Eds.; John Wiley and Sons, Ltd, 2011; pp 1153–1236.

(42) Herzberg, G. *Molecular Spectra and Molecular Structure: III. Electronic Spectra and Electronic Structure of Polyatomic Molecules*; D. Van Nostrand Company, 1966.

(43) Polanyi, J. C.; Woodall, K. B. Mechanisms of Rotational Relaxation. *J. Chem. Phys.* **1971**, *56*, 1563–1572.

(44) Procaccia, I.; Levine, R. D. Vibrational Energy Transfer in Molecular Collisions: An Information Theoretic Analysis and Synthesis. *J. Chem. Phys.* **1975**, *63*, 4261–4279.

(45) Den, T. S.; Frey, H. M.; Felker, P. M.; Leutwyler, S. Rotational Constants and Structure of $para$-Difluorobenzene Determined by Femtosecond Raman Coherence Spectroscopy: A New Transient Type. *J. Chem. Phys.* **2015**, *143*, 144306–1–12.

(46) Bak, K. L.; Gauss, J.; Jørgensen, P.; Olsen, J.; Helgaker, T.; Stanton, J. F. The Accurate Determination of Molecular Equilibrium Structures. *J. Chem. Phys.* **2001**, *114*, 6548–6556.

(47) Pawłowski, F.; Jørgensen, P.; Olsen, J.; Hegelund, F.; Helgaker, T.; Gauss, J.; Bak, K. L.; Stanton, J. F. Molecular Equilibrium Structures from Experimental Rotational Constants and Calculated Vibration-Rotation Interaction Constants. *J. Chem. Phys.* **2002**, *116*, 6482–6496.

(48) Demaison, J. Experimental, Semi-Experimental and *Ab Initio* Equilibrium Structures. *Mol. Phys.* **2007**, *105*, 3109–3138.

(49) Demaison, J.; Rudolph, H. D.; Császár, A. G. Deformation of the Benzene Ring upon Fluorination: Equilibrium Structures of all Fluorobenzenes. *Mol. Phys.* **2013**, *111*, 1539–1562.

(50) Harmony, M. D. The Equilibrium Carbon Carbon Single-Bond Length in Ethane. *J. Chem. Phys.* **1990**, *93*, 7522–7523.

Table 1: Pseudorotational and Radial Vibrational Populations of Cyclopentane at $T = 90K$ and $295K$.

Level	Quantum nos. r	l	Degeneracy	Energy [cm^{-1}]	$90K$ [%]	$295K$ [%]
$v = 0$	0	0	1	0.0	11.8	5.2
ν_{ps}	0	1	2	2.8	22.5	10.3
$2\nu_{ps}$	0	2	2	11.2	19.7	9.9
$3\nu_{ps}$	0	3	2	25.2	15.8	9.2
$4\nu_{ps}$	0	4	2	44.8	11.5	8.4
$5\nu_{ps}$	0	5	2	70.0	7.7	7.4
$6\nu_{ps}$	0	6	2	100.8	4.7	6.4
$7\nu_{ps}$	0	7	2	137.2	2.6	5.3
$8\nu_{ps}$	0	8	2	179.2	1.3	4.4
$9\nu_{ps}$	0	9	2	226.8	< 1	3.4
$10\nu_{ps}$	0	10	2	280.0	< 1	2.7
$11\nu_{ps}$	0	11	2	338.8	< 1	2.0
$12\nu_{ps}$	0	12	2	403.2	< 1	1.5
$13\nu_{ps}$	0	13	2	473.2	< 1	1.0
ν_{23}	1	0	1	273.0	< 1	1.4
$\nu_{23}+\nu_{ps}$	1	1	2	275.8	< 1	2.7
$\nu_{23}+2\nu_{ps}$	1	2	2	284.2	< 1	2.6
$\nu_{23}+3\nu_{ps}$	1	3	2	298.2	< 1	2.4
$\nu_{23}+4\nu_{ps}$	1	4	2	317.8	< 1	2.2
$\nu_{23}+5\nu_{ps}$	1	5	2	343.0	< 1	2.0
$\nu_{23}+6\nu_{ps}$	1	6	2	373.8	< 1	1.7
$\nu_{23}+7\nu_{ps}$	1	7	2	410.2	< 1	1.4
$\nu_{23}+8\nu_{ps}$	1	8	2	452.2	< 1	1.2

Table 2: Experimental and Calculated Rotational, Pseudorotational and Centrifugal Distortion Constants of Cyclopentane.

			CCSD(T)/cc-pVTZ		
Parameter	Reference 10	fs-DFWM	Planar D_{5h}	Bent (C_s)	Twist (C_2)
A_e / MHz			6416.875	6564.26	6563.425
B_e / MHz			6416.875	6558.76	6559.60
A_0 /MHz			6353.00	6520.46	6468.85
B_0 / MHz			6353.00	6459.27	6511.400
$(A_0 + B_0)/2$			6353.00	6489.87	6490.125
B_0 / MHz	6476 (3)	6484.93(1)	6353.00	6489.985	
$\alpha^B_{e,ps}$/ MHz	-	-0.000704(14)	3.273[1]	-0.937[1]	-0.538[1]
$\alpha^B_{e,23}$ / MHz	-	-9.542(66)	3.273[1]	-9.792[1]	-9.869[1]
D_J / kHz	1.5(4)	1.76(25)	1.637[2]	1.814[2]	1.817[2]
D_{JK} / kHz	-	-1.65(23)	-2.368[2]	29.128[2]	-1.686[2]

[1] calculated at the MP2/cc-pVTZ level

[2] D_J and D_{JK} constants for the excited vibrations are set to the $v = 0$ value.

Table 3: Calculated energies of cyclopentane conformers (in cm^{-1}) relative to that of the C_2 Twist form.

	MP2		CCSD(T)	
	cc-pVDZ	cc-pVTZ	cc-pVDZ	cc-pVTZ
D_{5h} Planar	2311.09	2311.16	2078.83	2100.53
C_s Bent	0.87	3.83	0.76	0.05

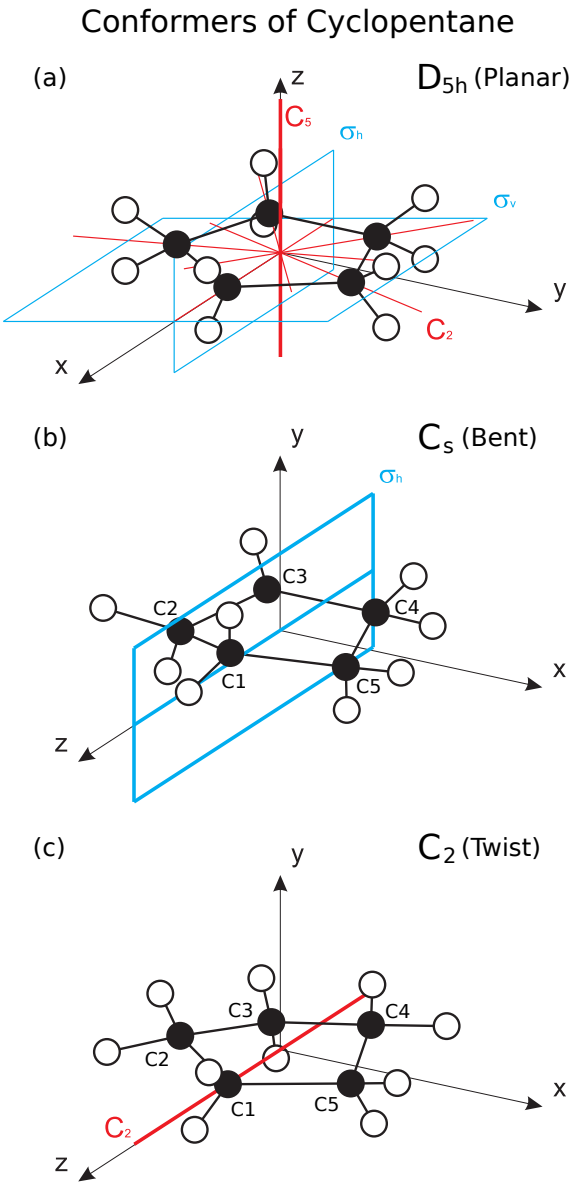

Figure 1: Conformers of cyclopentane: (a) the high-energy D_{5h} symmetric planar conformation, (b) one of the 10 C_s symmetric *Bent* conformations corresponding to the 10 minima in Fig. 2, (c) one of the 10 C_2 symmetric *Twist* conformations corresponding to the 10 potential maxima in Fig. 2

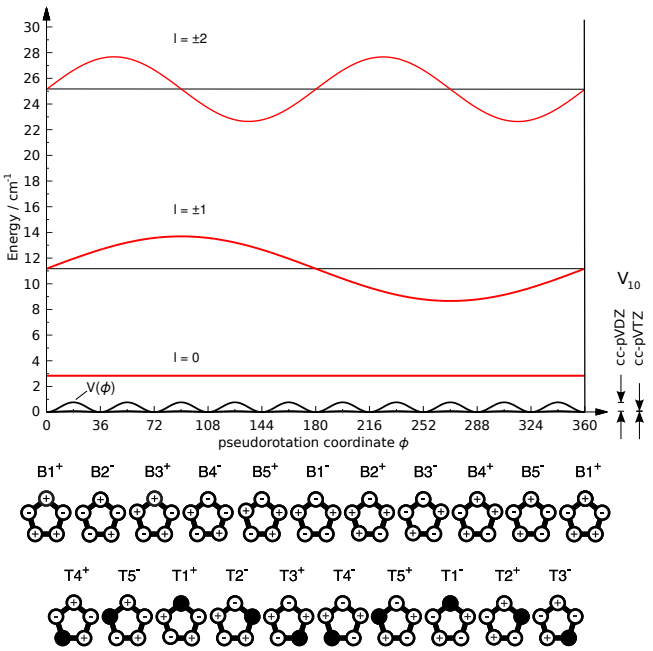

Figure 2: One-dimensional 10-fold cyclic potential energy curve $V(\phi)$ of cyclopentane. The ten *Bent* conformers and *Twist* conformers corresponding to the 20 stationary points are drawn schematically under the graph at the corresponding 20 distinct positions along the ϕ coordinate. The three lowest pseudorotational wave functions with quantum numbers $|l| = 0, 2$ and 3 are shown in red.

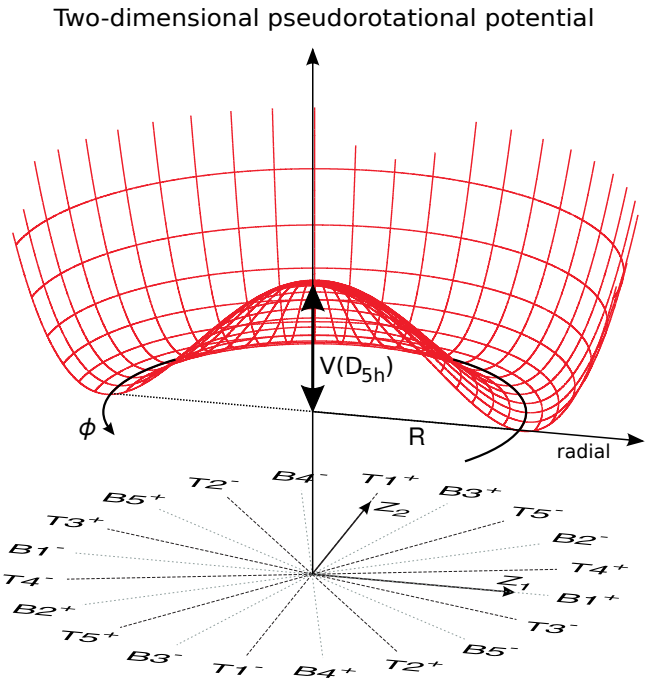

Figure 3: Two-dimensional potential energy surface of cyclopentane, $V(\phi, R)$, as a function of the pseudorotational coordinate ϕ and radial coordinate R. The positions of the 20 distinct conformers of cyclopentane along the ϕ coordinate are plotted beneath the PES.

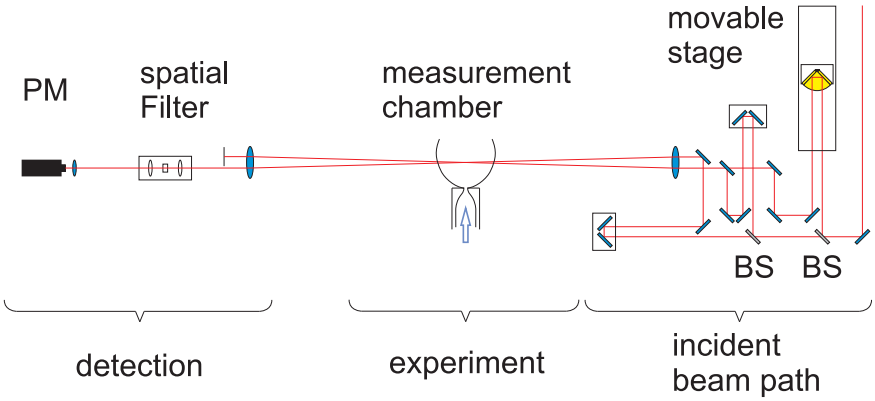

Figure 4: Schematic of the fs rotational Raman coherence spectroscopy setup. The fs seed laser and amplifier are not shown. On the right, the fs laser beam is split into pump, dump and probe beams (BS= beam splitter). using two beamsplitters. The three beams are overlapped and focussed into the core of the pulsed supersonic jet inside the vacuum chamber. the actual experiment. This generates the signal beam which is spatially filtered and detected by a photomultiplier. For details, see the Supporting Information.

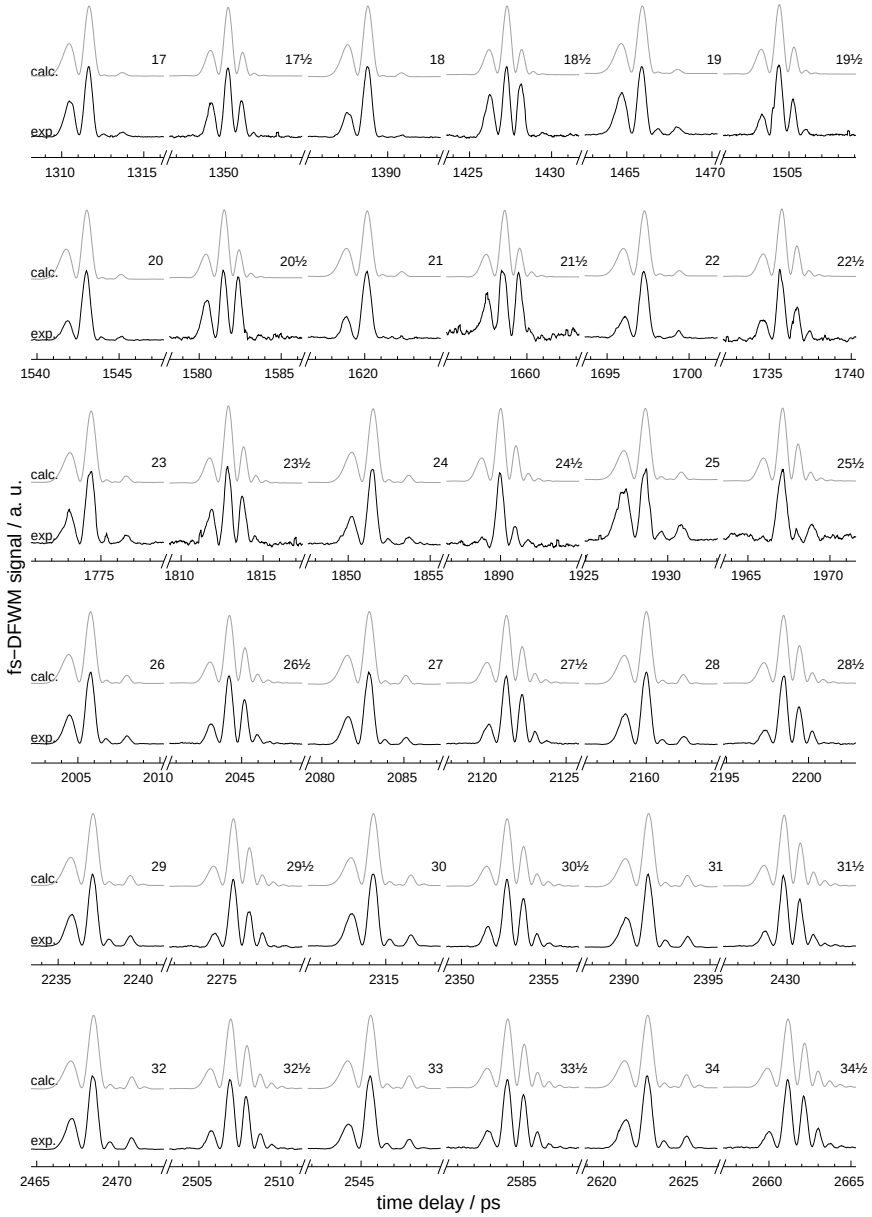

Figure 5: Rotational Raman RCS coherences transient of supersonic jet-cooled cyclopentane over the range of 1305-2665 ps (in black). The corresponding RCS simulation (in grey) employs the molecular parameters given in Table 2.

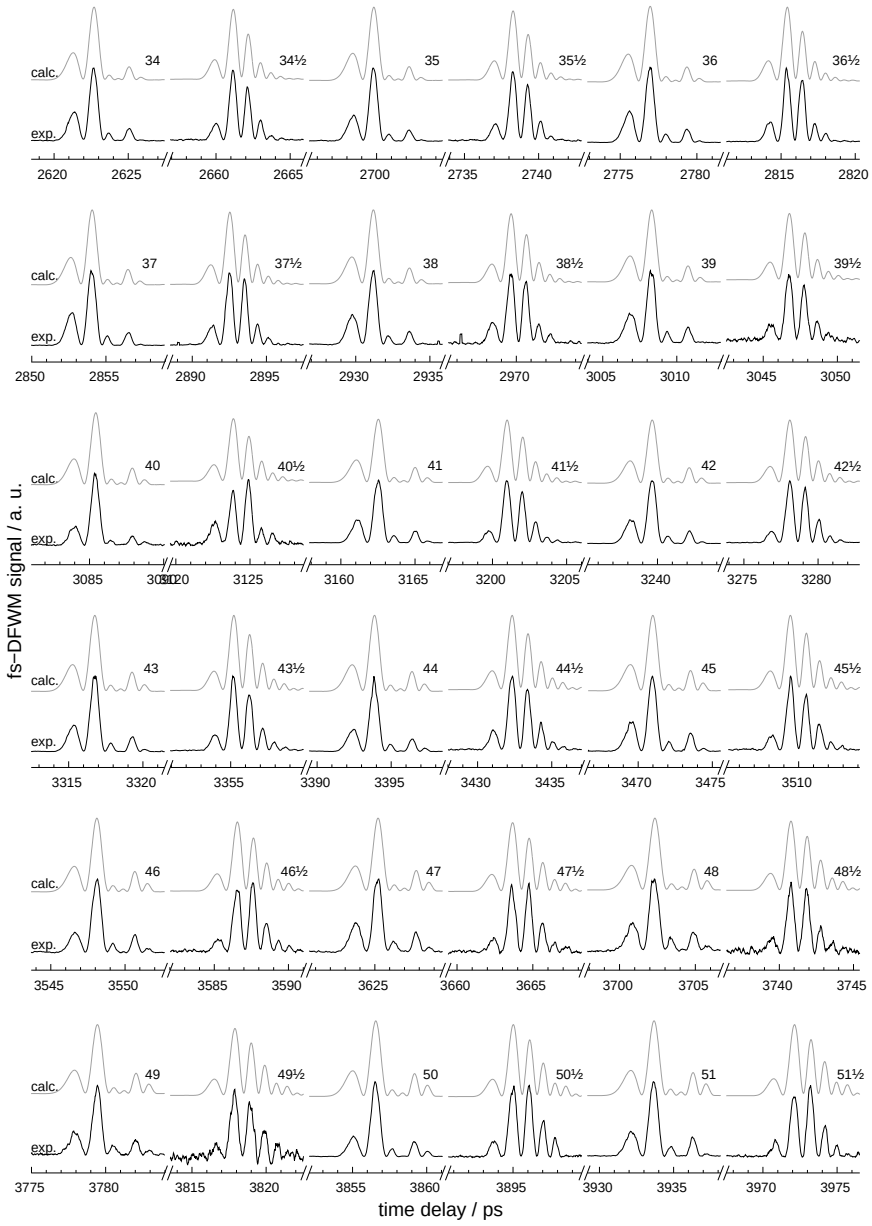

Figure 6: Continuation of Figure 5 over the range of 2618-3976 ps .

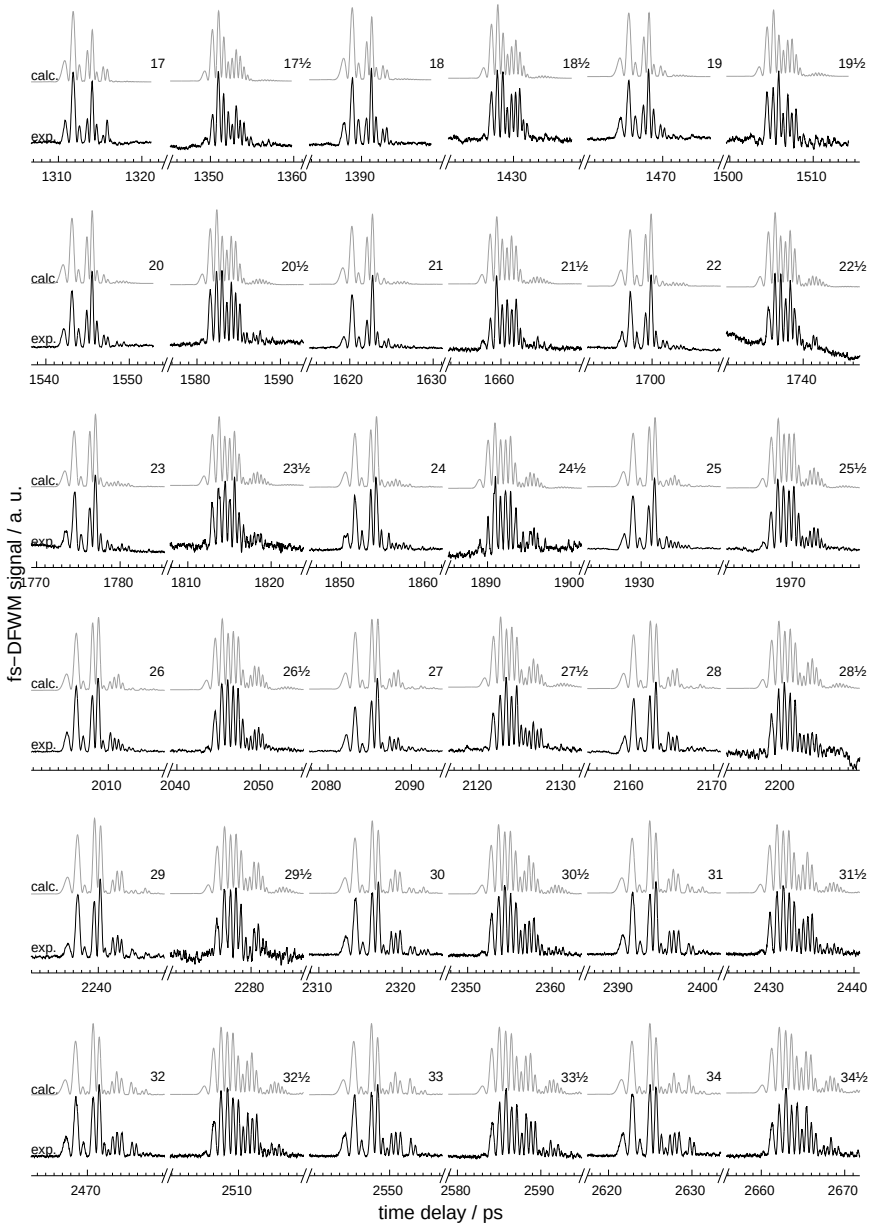

Figure 7: Rotational Raman RCS transients of cyclopentane in a gas cell at $T = 293$ K, over the range of 1317-2671 ps (in black). The corresponding simulation (in grey) employs the molecular parameters given in Table 2.

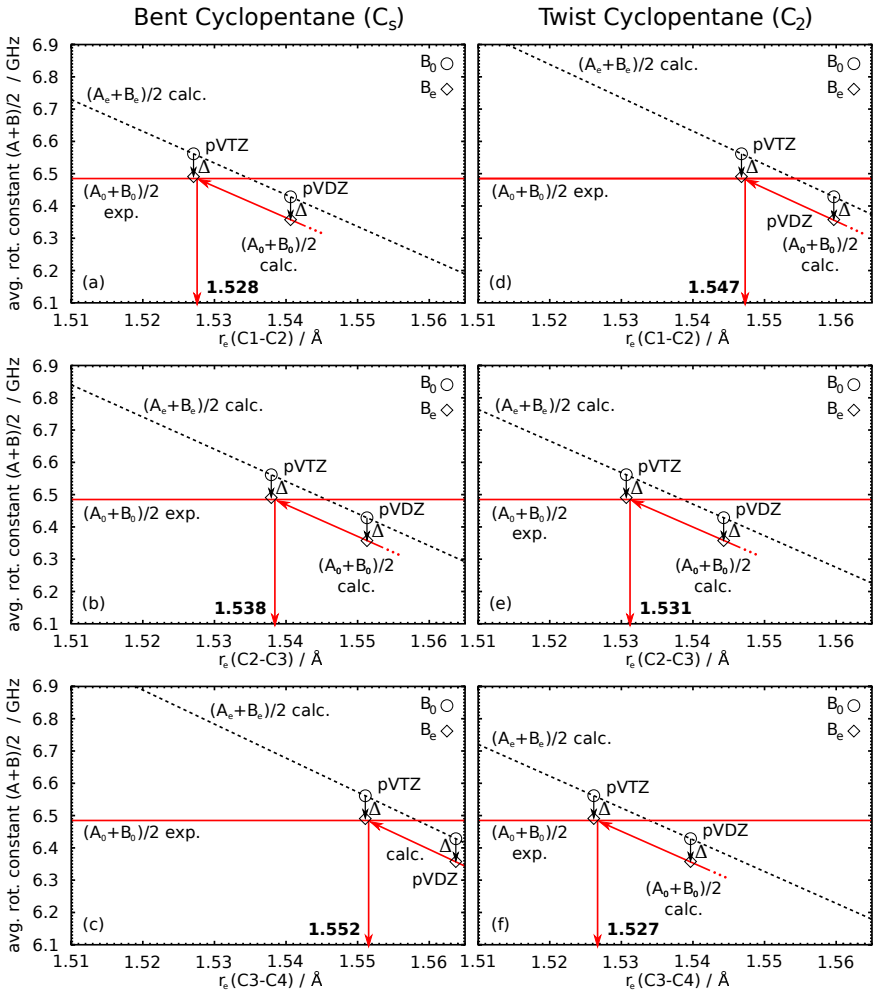

Figure 8: Calculated C-C bond lengths of the three distinct C-C bonds of Bent and Twist conformers of cyclopentane, calculated at the CCSD(T) level with the cc-pVDZ and cc-pVTZ basis sets.

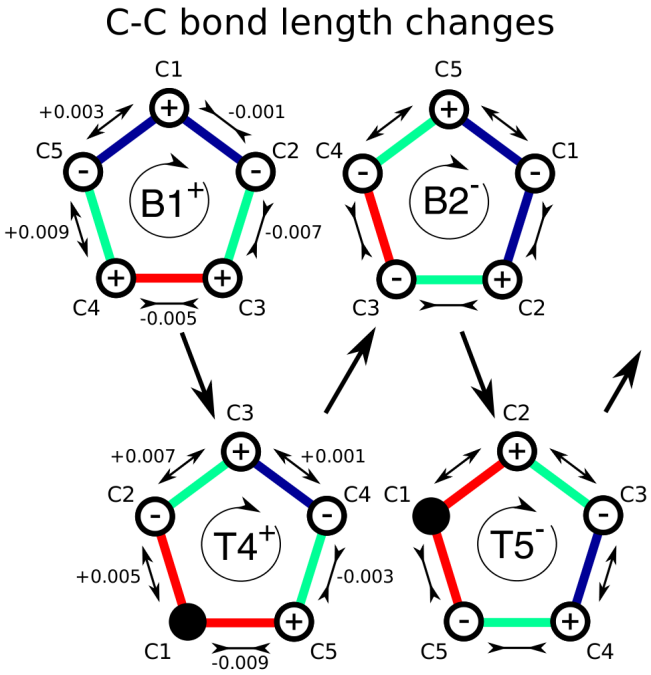

Figure 9: Scheme showing the changes of individual C-C bond lengths that occur during the first four pseudorotation steps that are shown in Figure 2. The "long" C-C bonds are color-coded in red, the "medium" C-C bonds in green and the "short" C-C bands in blue. The bond length expansions or contractions that occur on going from a given structure to the next are coded by double-headed arrows at the periphery of the C-C bonds.

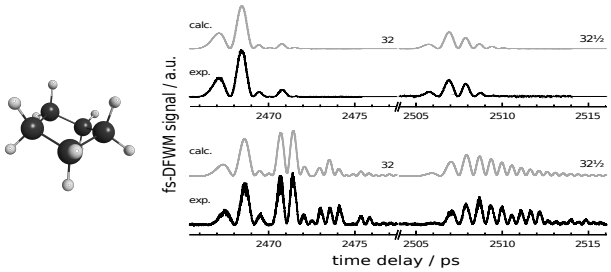

Figure 10: TOC graphic.